Measurements of the electron-impact differential cross sections and generalized oscillator strengths for excitation of the $2\,^1S$ and $3\,^1S$ states in helium at small scattering angles

T. Y. Suzuki, H. Suzuki, F. J. Currell, and S. Ohtani
Institute for Laser Science, University of Electro-Communications, Chofu-shi, Tokyo 182, Japan

Y. Sakai,* T. Takayanagi, and K. Wakiya
Department of Physics, Sophia University, Chiyoda-ku, Tokyo 102, Japan

(Received 25 August 1997)

Differential cross sections (DCS's) for excitation of the $2\,^1S$ and $3\,^1S$ states in helium have been measured at small scattering angles from 0° to 15° for the electron-impact energies from 100 to 500 eV. Measurements were performed with a high angular resolution, better than 1°, and with an accuracy of the angle position of 0.2°. Distinct forward peaking features have been observed at minute scattering angles lower than about 3° for impact energies higher than 200 eV. Experimental DCS's as functions of the scattering angle are compared with theoretical calculations based on various kinds of approximation method. Effective generalized oscillator strengths (GOS's) for the $2\,^1S$ and $3\,^1S$ excitations were deduced from the DCS's for impact energies 100–500 eV as a function of the squared momentum transfer K^2. A systematic discrepancy between the measured effective GOS's and the theoretical GOS calculated by the first Born approximation has been displayed at the low limit of K^2. The effective GOS's appear to approach the theoretical GOS very slowly as the impact energy increases, however, the GOS for low values of K^2 still does not agree with the theoretical GOS up to the impact energy 800 eV for the $2\,^1S$ excitation. [S1050-2947(98)03503-3]

PACS number(s): 34.80.Dp

I. INTRODUCTION

Studies on the electron-impact excitation of the $2\,^1S$ and the $3\,^1S$ states from the ground $1\,^1S$ state in He atoms are interesting because these processes are typical examples of transitions between the states for which the term symbols are the same for the initial and the final states.

Experimental studies on differential cross sections (DCS's) for excitation of the $2\,^1S$, $2\,^1P$, and other states in He were performed most actively during the early period of the development of electron-energy-loss spectroscopy for intermediate and high impact energies. Measurements of the DCS's for excitation of the $2\,^1S$ state in He have been carried out by Silverman and Lassettre for the incident energy $E_i = 500$ eV at scattering angles 4.73°–15.3° [1], and by Skerbele and Lassettre at angles $\theta = 0.5° - 2.5°$ [2]. Vriens, Simpson, and Mielczarek have measured the DCS's for $E_i = 100 - 500$ eV at $\theta = 5°$, 10°, and 15° [3], and Chamberlain, Mielczarek, and Kuyatt have performed absolute measurements of the DCS's for $E_i = 50 - 500$ eV at $\theta = 5°$ [4]. Takayanagi and co-workers measured the DCS's for $E_i = 50 - 500$ eV at $\theta = 20° - 120°$ [5–7]. Dillon and Lassettre measured the DCS's for the energy range $E_i = 200 - 700$ eV at the angles $\theta = 7.5° - 35°$ [8].

Subsequently, many measurements of the DCS's for the $2\,^1S$ excitation have been published, however, they were performed mainly for lower impact energies. Among these measurements, the results of Trajmar for the impact energies 29.6 and 40.1 eV [9] are worthy of special mention because he found a striking feature in the angular dependence of the DCS which has a deep minimum at an angle of around 50°.

Trajmar, Register, Cartwright, and Csanak have published results of the DCS's for the $2\,^1S$ and $3\,^1S$ excitation for the impact energies 30, 50, and 100 eV at scattering angles in the range 10°–135° [10]. Recently, Xu, Feng, Wu, Ji, Zhang, Zhong, and Zheng have measured the DCS's for the $2\,^1S$ excitation for the impact energy 1500 eV at the angles from 2° to 11.5° to determine the generalized oscillator strength (GOS) [11].

The experimental results, for intermediate and high impact energies, were treated mainly in the framework of the generalized oscillator strength based upon the Born approximation [12]. It is known that the Born approximation does not hold for excitation processes like the $1\,^1S \rightarrow 2\,^1S$ transition where the term symbols are the same in the initial and the final states even if the impact energies of electrons are in the range 300–500 eV [13,14]. This feature has also been observed experimentally in the case of the $X\,^1\Sigma_g^+ \rightarrow a''\,^1\Sigma_g^+$ in N_2 [14], and the $X\,^1\Sigma^+ \rightarrow B\,^1\Sigma^+, C\,^1\Sigma^+$ in CO [15].

It is well known that the DCS's for the excitation of the $2\,^1S$ state which are calculated by the first Born approximation are generally too small at large scattering angles. The theoretical DCS curve as a function of the scattering angle, for instance for the impact energy 500 eV, departs from experimental data at about 20°, and becomes one order of magnitude smaller than experimental data at 40°.

At minute scattering angles, very few experimental data are available on the DCS's for excitation of the $2\,^1S$ state in He except for one example of measurements by Skerbele and Lassettre [2]. On the other hand, plenty of theoretical studies have been published on the DCS's for the $2\,^1S$ excitation, which were calculated utilizing various types of approxima-

*Present address: Department of Physics, Toho University, Miyama, Funabashi, 274 Chiba, Japan.

tion method. A comprehensive review has been published on theoretical works for the DCS for excitation of He [16].

As for the behavior of the DCS's at minute scattering angles for intermediate and high impact energies, significant discrepancies are found depending on the type of method used. The first Born approximation results in the smallest value in the DCS at 0° angle [17]. The Glauber approximation also generally leads to the second smallest results at 0° angle [18]. Sophisticated calculation methods which consider higher-order terms and many-state basis generally lead to larger DCS's at the smallest angles. For instance, a calculation by means of the eikonal Born series method by Byron and Joacham [19] shows a considerable increase in the DCS's at small angles. The second-order potential theory by Berrington, Bransden, and Coleman [20] and the multichannel eikonal theory with the dipole correction by Mansky and Flannery show a forward peaking feature in the DCS's [21]. The *R*-matrix method using a five-state basis by Fon, Berrington, and Kingston gives the largest DCS at 0° angle [22]. The discrepancy in the values of the DCS at 0° angle among the theoretical results of different approximation methods amounts to about a factor of 5.

No experimental data have yet been made available to verify the validity of the theoretical calculations. It is a purpose of the present work to supply a series of experimental data of the DCS's for excitation of the $2\,^1S$ and $3\,^1S$ states in He at minute scattering angles in the intermediate and high impact energy region.

In this work, we present the experimental results of the DCS's for excitation of the $2\,^1S$ and $3\,^1S$ states from the ground state in He at scattering angles from 0° to 15° for impact energies 100, 200, 300, 400, and 500 eV. Conventional electron-energy-loss spectroscopy (EELS) has been used. However, we have paid special attention to the calibration of the scattering angle to determine the true angular scale and to maintain good angular resolution. Furthermore, we have taken consideration of the finite angular resolution in our analysis of the measured data.

The experimental DCS's were compared with theoretical calculations as functions of scattering angle for impact energies 100, 200, and 500 eV. The effective, or apparent, generalized oscillator strengths were deduced as functions of the squared momentum transfer K^2 from the DCS's for the $2\,^1S$ and the $3\,^1S$ excitations, and are displayed together with the theoretical GOS's calculated by the first Born approximation. This set of curves of the dependence of the effective GOS on the impact energy might be useful to display the character of transitions where the term symbols are the same in the initial and final states.

At low scattering angles, due to the finite angular resolution associated with any measurement, the measured scattering angle may differ by a significant amount from the mean scattering angle. Throughout this paper, unless the specific phrase ''the mean scattering angle'' is used, we refer to ''the measured angle'' as the geometrically measured scattering angle, corrected for systematic errors as described below.

II. EXPERIMENTAL APPARATUSES AND PROCEDURES

We used two sets of apparatus for the present measurements. The first one is an electron-impact spectrometer in the Institute for Laser Science, University of Electro-Communications, which we used for the measurements at 300 and 400 eV and at other energies, for scattering angles above 3°. This apparatus has been utilized for a series of measurements of DCS and GOS for the lowest excited states in rare-gas atoms, Ar [23], Kr [24], Xe [25,26], and Ne [27]. A detailed description of this apparatus has already been given [23].

The second electron spectrometer at Sophia University was used for the remaining measurements. This apparatus was designed especially to be suitable for measurements at minute angles including 0°. A brief description of this apparatus has already been given in a previous paper which reported the measurements on DCS's for the $2\,^3S$ state in He [28].

In order to make this paper self-contained, we will describe the construction and specifications of the two spectrometers briefly including subsequent improvements. The first spectrometer consists of an electron gun, an energy selector, a collision region, an energy analyzer, and a channel electron multiplier. A set of electrostatic lenses connects each part. Simulated hemispherical analyzers, first designed by Jost [29] are employed for the selector and analyzer. The mean trajectory radius is 50 mm for the selector and 80 mm for the analyzer. The energy selector is rotatable around the collision center from $-5°$ to $+110°$.

The whole electrode system of the spectrometer was covered by a cylindrical magnetic shield made of high magnetic permeability alloy (Permalloy PC), while the vertical component of the earth's magnetic field was canceled utilizing a pair of square Helmholtz coils. Consequently, the residual magnetic field at the spectrometer system was reduced to less than a few mG.

At the collision center, a target atomic beam was crossed with the electron beam at right angles. The target atomic beam effused from a nonmagnetic needle of 0.5 mm inner diameter and 10 mm length. The whole system was enclosed in a vacuum chamber where the ultimate pressure was about 1×10^{-7} Torr. The pressure when the EELS measurements were performed was maintained at less than 1×10^{-5} Torr.

The conventional constant resolution mode, where the deceleration voltage for the scattered electrons was swept keeping the pass energy through the analyzer constant, was used and the typical energy resolution was better than 50 meV [full width at half maximum (FWHM)].

The angular resolutions of the apparatuses have been estimated from the measurement of the angular distribution of the primary electron beam incident from the selector as a function of the rotation angle around 0° position. The angular resolutions were estimated to be 0.4° and 1.1° full width at half maximum for the two apparatuses used.

The second apparatus is an electron spectrometer which has essentially the same composition as the first one. This spectrometer, however, has been designed to make measurements at minute scattering angles including 0° angle, and for high impact energies. The most important difference is the use of tandem analyzers. Simulated hemispherical analyzers of the Jost type, with a mean radius of 52 mm, are employed for the energy selector and each component of the tandem-type analyzer. The energy analyzer is rotatable around the collision center from $-30°$ to 100°.

The whole of the selector and analyzer system is covered by a cylindrical magnetic shield made of Permalloy PC alloy, resulting in the residual magnetic fields being less than a few mG. All of these components are enclosed in a vacuum chamber evacuated with a turbomolecular pump, and the ultimate vacuum pressure was lower than a few times 10^{-7} Torr. The pressure during the EELS measurements was maintained below 1×10^{-5} Torr.

A set of apertures of 0.5 mm diameter was placed in the lens system before the analyzer to obtain the desired angular resolution. The electron-energy-loss spectra were measured utilizing the conventional constant resolution mode, and the typical energy resolution was better than 80 meV (FWHM).

Use of the tandem analyzer has proved to be effective to suppress background noise due to the multiple scattering of incident electrons on the inner surface of the outer hemisphere and the outer surface of the inner hemisphere of the analyzer. The tandem analyzer has enabled us to measure the EELS at 0° angle with sufficient signal-to-noise ratio to determine the intensity ratio $(I_{2\,^1S}/I_{2\,^1P})$ with an accuracy of about 5–7 %.

A nozzle of 0.5 mm diameter and 10 mm length was used to make an atomic beam, with which the impact electron beam collides at right angles, at the collision center. Calibration of the scattering angle scale was performed by use of the symmetrical nature of the scattering intensity ratio $(I_{2\,^1S}/I_{2\,^1P})$ in He. Figure 1(a) shows that the true 0° of the measured scattering angle scale is shifted by 0.5° to the positive side of the geometric zero angle of the instrument. Accuracy in the angle position is estimated to be better than 0.2°. The angular resolution is estimated from the measurement of the angular distribution of the incident electron beam from the selector as a function of rotation angle around 0° as shown in Fig. 1(b) to be about 1.1° (FWHM) for this second spectrometer.

For each spectrometer, under each set of experimental conditions, a calibration of the zero of scattering angle free from systematic errors has been performed, as described above.

For each energy loss spectrum the range of collection energies covered was much less than the mean collection energy. Furthermore, in both electron spectrometers, the energy-loss spectra were measured under conditions where the chromatic aberration in the electron lens before the analyzer was minimized, and consequently the peak intensity ratios should be proportional to the true ratios of the corresponding DCS's.

The results of the intensity ratio for each angle and each impact energy have been determined from an average of the intensity ratios obtained from three independent spectra measured at the same angle and for the same impact energy. The standard deviation in the measured ratios was at most 7%.

The absolute DCS's for the $2\,^1S$ excitation $(d\sigma/d\Omega)_{2\,^1S}$ were deduced from the scattering intensity ratio $(I_{2\,^1S}/I_{2\,^1P})$ utilizing the absolute DCS's for the $2\,^1P$ excitation $(d\sigma/d\Omega)_{2^1P}$ as the normalization standard, following the relationship

$$\left(\frac{d\sigma}{d\Omega}\right)_{2\,^1S}=\left(\frac{I_{2\,^1S}}{I_{2\,^1P}}\right)\left(\frac{d\sigma}{d\Omega}\right)_{2\,^1P}, \tag{1}$$

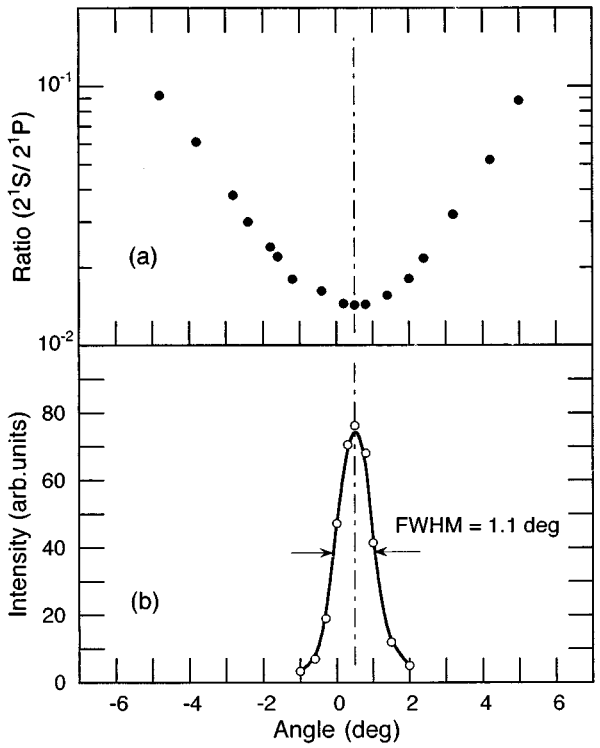

FIG. 1. (a) Calibration of the zero angle position. The vertical axis represents the intensity ratio $(I_{2\,^1S}/I_{2\,^1P})$ and the horizontal axis represents the geometric angle of the instrument. The symmetry nature of the scattering intensity ratio shows that the true zero degree of the scattering angle is shifted to $+0.5°$. (b) Typical angular distribution of the electron beam that is directly incident from the energy selector at the geometric zero angle. The angular resolution is estimated to be 1.1° (FWHM). The incident electron energy is 500 eV.

where $I_{2\,^1S}$ and $I_{2\,^1P}$ are the scattering intensities which were obtained by the corresponding peak area in the energy-loss spectra for the $2\,^1S$ and $2\,^1P$ excitation, respectively.

The absolute DCS's for the $2\,^1P$ excitation, which are considered to be the most reliable, were obtained from the following way. We adopted the DCS's $(d\sigma/d\Omega)_{2\,^1P}$ for $E_i \geqslant 300$ eV and $\theta \leqslant 15°$, which are calculated from the generalized oscillator strength $F(K)$ with the relationship [12]

$$\left(\frac{d\sigma}{d\Omega}\right)=\frac{2}{WK^2}\left[\frac{k_f}{k_i}\right]F(K), \tag{2}$$

where W is the excitation energy, k_i and k_f are the momenta of the colliding electrons before and after the collision, and K is the absolute value of the momentum transfer vector. All quantities are in atomic units. When the incident energy is E_i, excitation energy is W, and scattering angle is θ, k_i and k_f, and K are represented by the following relationship in atomic units:

$$k_i=\sqrt{2E_i}, \quad k_f=\sqrt{2(E_i-W)},$$

$$K^2=2(2E_i-W)-4\sqrt{E_i(E_i-W)}\cos\,\theta. \tag{3}$$

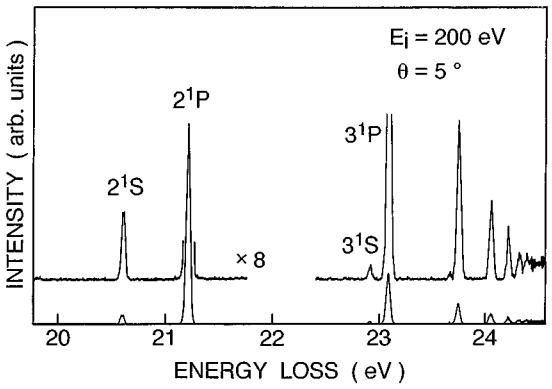

FIG. 2. A typical electron-energy-loss spectrum of He for the impact energy 200 eV at the scattering angle 5°, taken using the first electron spectrometer described in the main text.

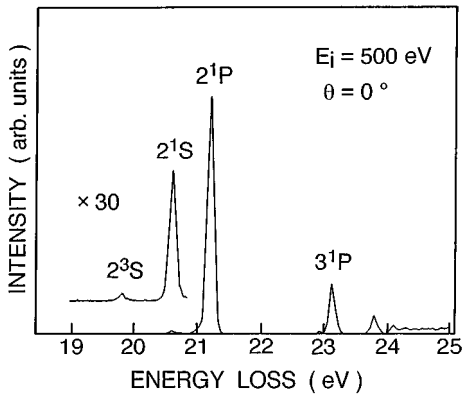

FIG. 3. A typical electron-energy-loss spectrum of He for the impact energy 500 eV at the scattering angle 0°, taken using the second electron spectrometer described in the main text.

The GOS $F(K)$ is related with the optical oscillator strength (OOS) f_0 using the expansion formula proposed by Dillon and Lassettre [8], which is independent of the validity of the Born approximation.

$$F(K)=\frac{1}{1+x^2}\left[f_0+\sum_{n=1}^{m} c_n\left\{\frac{x}{(1+x^2)^{1/2}}\right\}^n\right], \qquad (4)$$

where c_n are a series of coefficients, x is equal to K/Y, here Y is equal to $\sqrt{2I}+\sqrt{2(I-W)}$, while I and W are the ionization energy and excitation energy, respectively.

We obtained the c_n coefficients and hence DCS's for the $2\,^1P$ excitation from reference data using the least-squares method. We obtained the DCS's for the impact energy $E_i \geqslant 200$ eV fitting to the experimental data measured by Dillon and Lassettre [8] except for the impact energies 600–800 eV. At these energies, reference data were derived from the calculations of Kim and Inokuti [17].

For the impact energy $E_i=100$ eV, the coefficients were deduced from a fit to experimental data measured previously in our laboratory. The DCS's for the $2\,^1P$ excitation have been determined from the experimental ratio of the peak intensity for the $2\,^1P$ excitation compared to the elastic scattering peak ($I_{2\,^1P}/I_{\text{elastic}}$). The absolute values were deduced by multiplying the intensity ratio by experimental DCS's for the elastic scattering measured by Jansen *et al.* [30]. Results of the DCS's are in good agreement with those reported by Cartwright, Csanak, Trajmar, and Register [31] within the mutual experimental errors.

For measurements at low scattering angles, the angular resolution cannot be neglected. Using a procedure outlined in the Appendix, we determined the effect of the finite angular resolution and made appropriate corrections to both the cross section scale and the angular scale.

III. RESULTS AND DISCUSSION

A typical energy-loss spectrum in He is shown in Fig. 2, which was taken for the impact energy 200 eV and at the scattering angle 5°. An example of the energy-loss spectrum at a measured angle 0° is shown in Fig. 3 for the impact energy 500 eV.

A. DCS for the $2\,^1S$ excitation

Results of the measured intensity ratios ($I_{2\,^1S}/I_{2\,^1P}$) and the DCS's for the excitation of the $2\,^1S$ state $(d\sigma/d\Omega)_{2\,^1S}$ are tabulated in Table I against the measured scattering angles for the impact energies 100, 200, 300, 400, and 500 eV. The DCS's $(d\sigma/d\Omega)_{2\,^1P}$ for the $2\,^1P$ excitation, which were used as the normalization standards, are also listed. The squared momentum transfer K^2, and the effective generalized oscillator strength $F(K)$ are listed in the last two columns for comparison of the relationship of the DCS versus scattering angle with that of the $F(K)$ versus K^2.

In Table I, the DCS's for the $2\,^1P$ and $2\,^1S$ at the angles larger than 15° for the impact energies 100, 300, 400, and 500 eV, and those at the angles larger than 30° for the impact energy 200 eV are experimental data measured in the previous experiments in our laboratory performed over a wide range of scattering angles, part of which have already been published [5,6].

For Table I, the DCS's for the $2\,^1P$ excitation and the intensity ratios are not listed in the rows corresponding to angles larger than 30° for the impact energy 200 eV, and angles larger than 15° for the impact energies 300, 400, and 500 eV. The reason is as follows: the DCS's for the $2\,^1P$ excitation obtained in our previous measurement were systematically larger than those determined by Dillon and Lassettre at these large angles [8]. These excess values in the DCS's for the $2\,^1P$ excitation were pointed out by Dillon and Lassettre to be due to a pressure effect, which is caused by a combination of an elastic collision and an inelastic collision, one of which is in the forward direction [8]. For the DCS's for the $2\,^1S$ excitation, however, the listed data are in very good agreement with those of Dillon and Lassettre, where the pressure effect might be negligible.

For the DCS's for the $2\,^1P$ excitation for the impact energy 100 eV, the listed data agree well with those of Cartwright, Csanak, Trajmar, and Register [31], and those of Vriens, Simpson, and Mielczarek [3] renormalized to the absolute measurements at $\theta=5°$ by Chamberlain, Mielczarek, and Kuyatt [4], within the mutual experimental errors.

The experimental errors in the results of the DCS $(d\sigma/d\Omega)_{2\,^1S}$ at angles larger than 3° for all impact energies are estimated to be less than $\pm 11\%$, which is deduced as the quadratic sum of the statistical error 7% in the intensity ra-

TABLE I. The intensity ratios $(d\sigma/d\Omega)_{2\,^1S}/(d\sigma/d\Omega)_{2\,^1P}$ and the DCS's $(d\sigma/d\Omega)_{2\,^1S}$ (in atomic units) at impact energies 100, 200, 300, 400, and 500 eV. The absolute cross sections for the $2\,^1P$ excitation $(d\sigma/d\Omega)_{2\,^1P}$, which are used for the normalization standards, are also listed. The squared momentum transfer K^2 and the corresponding effective generalized oscillator strengths $F(K)$ are listed in the last two columns. The square brackets denote powers of 10.

Scattering angle (deg)	Intensity ratio $\frac{(d\sigma/d\Omega)_{2\,^1S}}{(d\sigma/d\Omega)_{2\,^1P}}$	$(d\sigma/d\Omega)_{2\,^1P}$ (a_0^2/sr)	$(d\sigma/d\Omega)_{2\,^1S}$ (a_0^2/sr)	Squared momentum transfer K^2	Effective GOS for $2\,^1S$ $F(K)$
		$E_i = 100$ eV			
1.2	5.18[−2]				
2.2	5.44[−2]				
2.7	5.53[−2]				
3.7	5.70[−2]	3.92	2.23[−1]	1.15[−1]	1.09[−2]
4.7	5.75[−2]	3.29	1.89[−1]	1.32[−1]	1.06[−2]
5.7	5.90[−2]	2.71	1.60[−1]	1.52[−1]	1.03[−2]
6.7	6.08[−2]	2.21	1.34[−1]	1.77[−1]	1.01[−2]
7.7	6.43[−2]	1.78	1.15[−1]	2.05[−1]	1.00[−2]
9.7	7.25[−2]	1.15	8.33[−2]	2.75[−1]	9.72[−3]
11.7	8.87[−2]	7.46[−1]	6.62[−2]	3.59[−1]	1.01[−2]
13.7	1.02[−1]	5.00[−1]	5.10[−2]	4.60[−1]	9.97[−3]
15	1.3 [−1]	3.3 [−1]	4.3 [−2]	5.3 [−1]	9.7 [−3]
20	1.9 [−1]	1.2 [−1]	2.3 [−2]	8.8 [−1]	9.0 [−3]
25	2.6 [−1]	4.8 [−2]	1.2 [−2]	1.3	6.1 [−3]
30	2.9 [−1]	1.8 [−2]	5.2 [−3]	1.8	4.0 [−3]
35	3.1 [−1]	1.1 [−2]	3.4 [−3]	2.5	3.4 [−3]
40	4.1 [−1]	6.5 [−3]	2.7 [−3]	3.2	3.3 [−3]
45	4.9 [−1]	3.6 [−3]	1.8 [−3]	3.9	2.8 [−3]
50	5.4 [−1]	2.7 [−3]	1.5 [−3]	4.8	3.0 [−3]
55	6.7 [−1]	2.0 [−3]	1.3 [−3]	5.7	3.1 [−3]
60	8.1 [−1]	1.5 [−3]	1.2 [−3]	6.6	3.4 [−3]
65	8.5 [−1]	1.6 [−3]	1.4 [−3]	7.6	4.2 [−3]
75	1.2	1.2 [−3]	1.5 [−3]	9.8	6.2 [−3]
85	1.3	8.0 [−4]	1.0 [−3]	1.2 [+1]	5.1 [−3]
		$E_i = 200$ eV			
0	3.01[−2]				
0.5	2.83[−2]				
1.0	2.71[−2]				
1.5	2.79[−2]				
2.2	2.50[−2]				
3.2	2.99[−2]	6.37	1.91[−1]	8.46[−2]	6.46[−3]
4.2	3.78[−2]	4.41	1.67[−1]	1.16[−1]	7.75[−3]
5.2	4.76[−2]	3.06	1.46[−1]	1.56[−1]	9.10[−3]
6.2	5.91[−2]	2.14	1.27[−1]	2.04[−1]	1.04[−2]
7.2	7.52[−2]	1.52	1.14[−1]	2.61[−1]	1.19[−2]
8.2	9.19[−2]	1.09	1.00[−1]	3.26[−1]	1.30[−2]
9.2	1.10[−1]	7.86[−1]	8.65[−2]	3.99[−1]	1.38[−2]
10.2	1.35[−1]	5.71[−1]	7.77[−2]	4.81[−1]	1.50[−2]
11.2	1.61[−1]	4.17[−1]	6.72[−2]	5.72[−1]	1.54[−2]
12.2	1.94[−1]	3.06[−1]	5.94[−2]	6.70[−1]	1.59[−2]
13.2	2.38[−1]	2.25[−1]	5.36[−2]	7.77[−1]	1.67[−2]
14.2	2.50[−1]	1.63[−1]	4.07[−2]	8.92[−1]	1.50[−2]
15.2	2.87[−1]	1.19[−1]	3.42[−2]	1.02	1.49[−2]
16.2	3.53[−1]	8.79[−2]	3.10[−2]	1.15	1.42[−2]
17.2	3.83[−1]	6.51[−2]	2.49[−2]	1.30	1.28[−2]
18.2	4.68[−1]	4.85[−2]	2.27[−2]	1.43	1.30[−2]
19.2	5.10[−1]	3.64[−2]	1.85[−2]	1.59	1.18[−2]
20.2	5.25[−1]	2.75[−2]	1.44[−2]	1.75	1.01[−2]
21.2	5.39[−1]	2.09[−2]	1.13[−2]	1.93	8.70[−3]
22.2	5.98[−1]	1.60[−2]	9.59[−3]	2.11	8.08[−3]
23.2	6.15[−1]	1.24[−2]	7.64[−3]	2.29	7.01[−3]

TABLE I. (*Continued.*)

Scattering angle (deg)	Intensity ratio $\frac{(d\sigma/d\Omega)_{2\,^1S}}{(d\sigma/d\Omega)_{2\,^1P}}$	$(d\sigma/d\Omega)_{2\,^1P}$ (a_0^2/sr)	$(d\sigma/d\Omega)_{2\,^1S}$ (a_0^2/sr)	Squared momentum transfer K^2	Effective GOS for $2\,^1S$ $F(K)$
30			2.8 [−3]	3.77	4.22[−3]
35			1.6 [−3]	5.08	3.25[−3]
40			1.1 [−3]	6.56	2.88[−3]
45			9.2 [−4]	8.20	3.02[−3]
55			7.3 [−4]	1.19[+1]	3.48[−3]
		$E_i = 300$ eV			
0.75	1.81[−2]	1.92[+1]	3.47[−1]	3.06[−2]	4.16[−3]
1.75	1.85[−2]	1.23[+1]	2.27[−1]	4.68[−2]	4.17[−3]
2.75	2.57[−2]	7.24	1.86[−1]	7.60[−2]	5.54[−3]
3.75	3.65[−2]	4.36	1.59[−1]	1.18[−1]	7.35[−3]
4.75	4.65[−2]	2.71	1.26[−1]	1.73[−1]	8.56[−3]
5.75	6.57[−2]	1.75	1.15[−1]	2.41[−1]	1.09[−2]
7.75	1.20[−1]	7.79[−1]	9.35[−2]	4.16[−1]	1.53[−2]
9.75	1.83[−1]	3.71[−1]	6.79[−2]	6.42[−1]	1.71[−2]
14.75	4.36[−1]	6.19[−2]	2.70[−2]	1.43	1.52[−2]
20			6.7 [−3]	2.59	6.82[−3]
25			2.3 [−3]	4.01	3.62[−3]
30			1.4 [−3]	5.73	3.15[−3]
40			8.6 [−4]	9.98	3.37[−3]
		$E_i = 400$ eV			
0.75	1.45[−2]	2.53[+1]	3.67[−1]	2.49[−2]	3.55[−3]
1.75	1.47[−2]	1.32[+1]	1.94[−1]	4.68[−2]	3.53[−3]
2.75	2.60[−2]	6.77	1.76[−1]	8.60[−2]	5.88[−3]
3.75	3.89[−2]	3.71	1.44[−1]	1.43[−1]	8.00[−3]
4.75	6.34[−2]	2.16	1.37[−1]	2.17[−1]	1.15[−2]
5.75	8.88[−2]	1.31	1.16[−1]	3.08[−1]	1.39[−2]
7.75	1.61[−1]	5.14[−1]	8.28[−2]	5.43[−1]	1.75[−2]
9.75	2.63[−1]	2.16[−1]	5.67[−2]	8.47[−1]	1.87[−2]
14.75	6.62[−1]	2.66[−2]	1.76[−2]	1.91	1.30[−2]
20			3.4 [−3]	3.47	4.59[−3]
30			8.3 [−4]	7.69	2.48[−3]
40			3.9 [−4]	1.34[+1]	2.04[−3]
		$E_i = 500$ eV			
0	1.45[−2]				
0.4	1.32[−2]				
0.8	1.43[−2]				
1.2	1.49[−2]				
1.8	1.95[−2]				
2.3	2.57[−2]				
2.8	3.30[−2]				
3.1	3.80[−2]	4.65	1.77[−1]	1.21[−1]	8.30[−3]
3.5	4.86[−2]	3.59	1.75[−1]	1.50[−1]	1.02[−2]
3.8	5.45[−2]	2.98	1.63[−1]	1.74[−1]	1.10[−2]
4.8	8.43[−2]	1.68	1.42[−1]	2.68[−1]	1.47[−2]
5.8	1.22[−1]	9.90[−1]	1.21[−1]	3.84[−1]	1.80[−2]
7.1	1.79[−1]	5.18[−1]	9.27[−2]	5.68[−1]	2.04[−2]
8.1	2.25[−1]	3.20[−1]	7.20[−2]	7.34[−1]	2.04[−2]
9.1	2.93[−1]	1.99[−1]	5.84[−2]	9.22[−1]	2.08[−2]
11.1	4.84[−1]	7.83[−2]	3.79[−2]	1.36	2.00[−2]
13.1	6.13[−1]	3.11[−2]	1.90[−2]	1.89	1.39[−2]
16			8.1 [−3]	2.80	8.79[−3]
21			2.3 [−3]	4.80	4.27[−3]
26			9.4 [−4]	7.30	2.65[−3]
31			5.3 [−4]	1.03[+1]	2.11[−3]
36			3.3 [−4]	1.38[+1]	1.76[−3]
41			2.6 [−4]	1.77[+1]	1.78[−3]

TABLE II. The DCS's $(d\sigma/d\Omega)_{2\,^1S}$ corrected for the limited angular resolution effects at small scattering angles, for impact energies 100, 200, 500, 600, 700, and 800 eV. Average angles and absolute DCS's $(d\sigma/d\Omega)_{2\,^1P}$ for the $2\,^1P$ excitation corrected for the angular resolution effects are also listed. The squared momentum transfer K^2 and the effective GOS's $F(K)$ are listed corresponding to the corrected average angle and the corrected DCS's $(d\sigma/d\Omega)_{2\,^1S}$, respectively. See the Appendix for details of notation used in the headings of the second and third columns.

Measured angle θ_m (deg)	Mean scattering angle $\overline{\theta(\theta_m)}$ (deg)	$\int S(\theta_m,\theta_t)\times\left(\frac{d\sigma}{d\Omega}(\theta_t)\right)_{2\,^1P} d\theta_t$ (a_0^2/sr)	$\left(\frac{d\sigma}{d\Omega}[\overline{\theta(\theta_m)}]\right)_{2\,^1S}$ (a_0^2/sr)	Squared momentum transfer K^2	Effective GOS for $2\,^1S$ $F(K)$
		$E_i=100$ eV			
1.2	1.25	4.98	2.55[−1]	9.04[−2]	9.80[−3]
2.2	2.20	4.57	2.49[−1]	9.70[−2]	1.03[−2]
2.7	2.70	4.34	2.40[−1]	1.02[−1]	1.04[−2]
		$E_i=200$ eV			
0.0	0.60	1.29[+1]	3.88[−1]	4.27[−2]	6.63[−3]
0.5	0.75	1.26[+1]	3.57[−1]	4.36[−2]	6.22[−3]
1.0	1.10	1.19[+1]	3.21[−1]	4.63[−2]	5.94[−3]
1.5	1.52	1.01[+1]	2.85[−1]	5.10[−2]	5.81[−3]
2.2	2.20	8.92	2.23[−1]	6.17[−2]	5.50[−3]
		$E_i=500$ eV			
0.0	0.60	3.157[+1]	4.58[−1]	1.99[−2]	3.53[−3]
0.4	0.70	2.983[+1]	3.94[−1]	2.13[−2]	3.25[−3]
0.8	0.95	2.580{+1]	3.69[−1]	2.58[−2]	3.68[−3]
1.2	1.25	2.093[+1]	3.11[−1]	3.30[−2]	3.93[−3]
1.8	1.8	1.387[+1]	2.70[−1]	5.14[−2]	5.37[−3]
2.3	2.3	9.42	2.42[−1]	7.39[−2]	6.92[−3]
2.8	2.8	6.43	2.12[−1]	1.02[−1]	8.36[−3]
		$E_i=600$ eV			
0.0	0.6	3.694[+1]	4.06[−1]	1.80[−2]	2.82[−3]
		$E_i=700$ eV			
0.0	0.6	4.023[+1]	3.58[−1]	1.71[−2]	2.35[−3]
		$E_i=800$ eV			
0.0	0.6	4.398[+1]	3.36[−1]	1.62[−2]	2.09[−3]

tios, systematic error 5% caused by the effect of the limited energy resolution, angular resolution and the angle calibration and others and the error 7% in the standard absolute values of the $2\,^1P$ DCS, $(d\sigma/d\Omega)_{2\,^1P}$.

When the DCS is a steep function of the angle in the forward direction, as in the case of the $1\,^1S\rightarrow 2\,^1P$ excitation for high impact energies, the measured angular dependence of the peak intensity may be changed due to the limited angular resolution of the spectrometer. Errors especially at the smallest scattering angles for high impact energies are mainly due to the uncertainty in the calibration of the scattering angle and the limited angular resolution of the apparatus.

The experimental uncertainty in the DCS $(d\sigma/d\Omega)_{2\,^1S}$ at 0° without any correction is estimated to be -22%, and $+11\%$, for the impact energies higher than 500 eV, which is deduced as the quadratic sum of the statistical error 9%, a systematic error -20%, $+5\%$, due to the effect of the limited angular resolution, and the error of 3% in the standard DCS $(d\sigma/d\Omega)_{2\,^1P}$. For the DCS $(d\sigma/d\Omega)_{2\,^1S}$ for which a correction has been applied, the typical error is estimated to be about 15%. The correction was applied to all data for which its magnitude was comparable to the systematic uncertainties. The corrected entries are given in Table II. Here, the DCS's for the $2\,^1S$ excitation, $(d\sigma/d\Omega)[\overline{\theta(\theta_m)}]_{2\,^1S}$, are expressed as a function of the mean scattering angle θ, which is calculated as the mean angle in the distribution function of the angular resolving power, which is in turn the function of the measured angle θ_m. The mean scattering angle θ, of course, becomes equal to θ_m at higher angles. Concerning the exact definition of θ, the reader should refer to the description in the Appendix.

Experimental uncertainty in the DCS's at angles larger than 15°, which have been adopted from the results of the previous experiments, is estimated to be about 15%, for which the main source of the error comes from the systematic and statistical errors in the determination of the intensity ratios, about 10%, due to the energy resolution and signal-to-noise ratio.

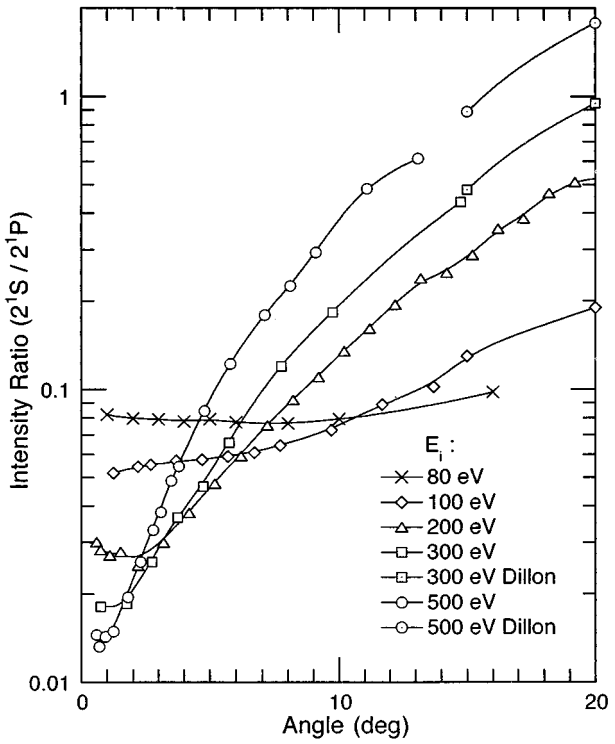

FIG. 4. Intensity ratio (I_{2^1S}/I_{2^1P}) in He as a function of the scattering angle for the impact energies $E_i = 80$, 100, 200, 300, and 500 eV.

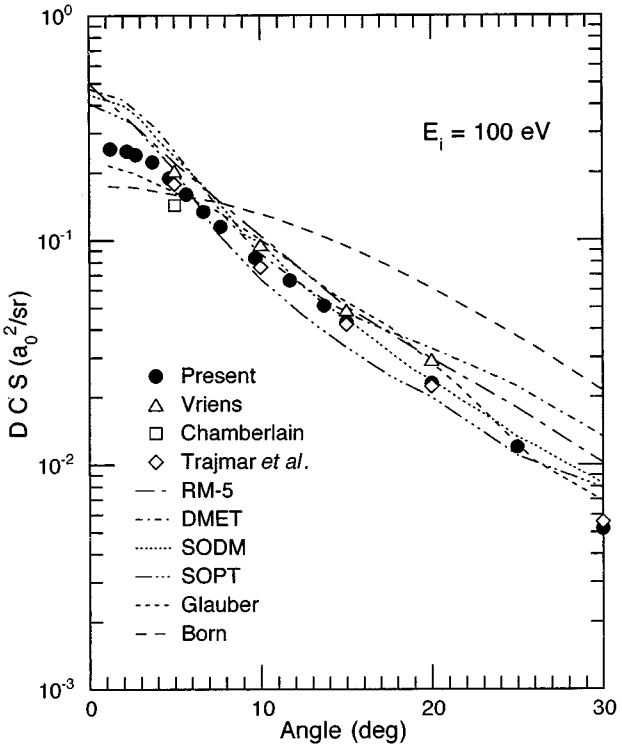

FIG. 5. The DCS's $(d\sigma/d\Omega)_{2^1S}$ in He as a function of the scattering angle for the impact energy $E_i = 100$ eV. Experimental data of Vriens, Simpson, and Mielczarek [3], Chamberlain, Mielczarek, and Kuyatt [4], and of Trajmar *et al.* [10] are also plotted. Results of the theoretical calculations are in the order of the DCS value at $\theta = 0°$; RM-5 of Fon, Berrington, and Kingston [22], DMET of Mansky and Flannery [21], SODM of Baye and Heenen [32], SOPT of Berrington, Bransden, and Coleman [20], Glauber of Franco [18], and Born of Kim and Inokuti [17]. Refer to the main text for the names of the calculation methods which correspond to the respective abbreviations.

The intensity ratios (I_{2^1S}/I_{2^1P}) for the different impact energies are shown in Fig. 4 as a function of the scattering angle. To avoid making the curves indistinct, data for $E_i = 400$ eV are not plotted but data for $E_i = 80$ eV are plotted for reference. For the impact energies from 200 eV to 500 eV, the intensity ratio decreases slowly as the angle decreases. This decrease becomes steeper as the angle decreases down to about 2°. At lower angles, the intensity ratio becomes constant or increases. For the impact energy 100 eV, the decrease in the ratio is very gentle and no increase at the near-zero angle is observed.

The DCS's $(d\sigma/d\Omega)_{2^1S}$ for $E_i = 100$ eV are shown in Fig. 5 on a logarithmic scale as a function of the scattering angle. Experimental data by Vriens, Simpson, and Mielczarek, which are not renormalized [3], are plotted together with data of Chamberlain, Mielczarek, and Kuyatt at $\theta = 5°$ [4], and recent data of Trajmar, Register, Cartwright, and Csanak [10]. The experimental data give a reasonable agreement with each other within experimental uncertainties.

Results of theoretical calculations using different approximation methods are shown for comparison to the experimental data. There are significant discrepancies among the different calculations. Starting with calculations which give the largest DCS, the five-state R-matrix method (RM-5) of Fon, Berrington, and Kingston [22], the dipole corrected multichannel eikonal theory (DMET) of Mansky and Flannery [21], the second-order diagonalization method (SODM) of Baye and Heenen [32], and the second-order potential theory (SOPT) of Berrington, Bransden, and Coleman [20], give the DCS's at 0° much greater than the experimental data. On the other hand, the Glauber approximation of Franco [18], and the first Born approximation of Kim and Inokuti [17], give smaller values at small angles. The first Born approximation gives a remarkable discrepancy from the experimental data and all other theoretical calculations. The experimental results do not display a distinct increase in the DCS's at the smallest angles in contrast to the prediction by the advanced calculations with higher-order terms and multichannel considerations.

The DCS's for the $2\,^1S$ excitation for the impact energy 200 eV are shown in Fig. 6 on a logarithmic scale as a function of the scattering angle. Experimental data of Dillon and Lassettre [8], those of Vriens, Simpson, and Mielczarek, which are not renormalized [3], and those of Chamberlain, Mielczarek, and Kuyatt [4] are also plotted together. Agreement among the experimental DCS's is very good.

Results of calculations (largest magnitude first) of the RM-5 of Fon, Berrington, and Kingston [22], the DMET of Mansky and Flannery [21], the SOPT of Berrington, Bransden, and Coleman [20], and the eikonal Born series method (EBSM) of Byron and Joachain [33], give larger DCS's near 0° angle. The RM-5 gives a value a factor of 2 larger at 0° compared with other calculations. The Glauber and the first Born approximations give smaller DCS's at 0° angle. The calculations with the higher-order terms and multichannel contributions reproduce a steep increase in the DCS's at the

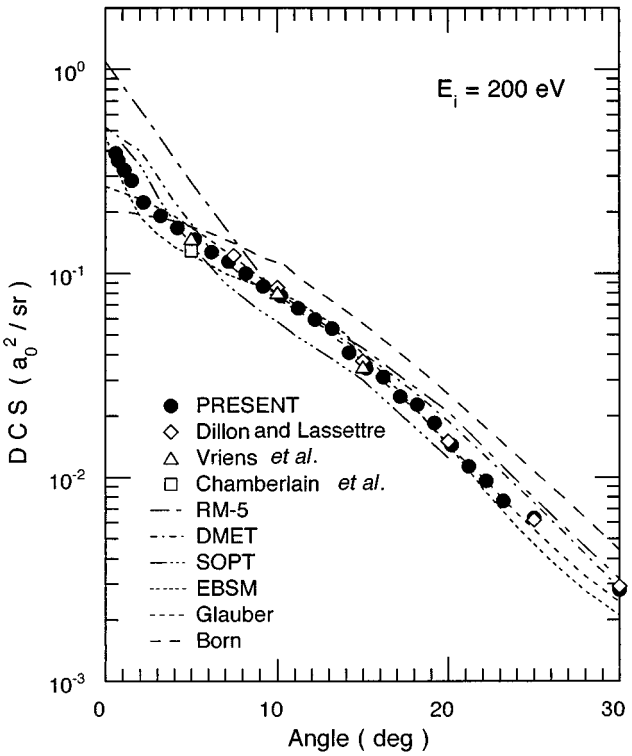

FIG. 6. The DCS's $(d\sigma/d\Omega)_{2\,^1S}$ in He as a function of the scattering angle for the impact energy $E_i = 200$ eV. Experimental data of Dillon and Lassettre [8] Vriens, Simpson, and Mielczarek [3], and Chamberlain, Mielczarek, and Kuyatt [4] are also plotted. Results of the theoretical calculations are in the order of the DCS value at $\theta = 0°$; RM-5 of Fon, Berrington, and Kingston [22], DMET of Mansky and Flannery [21], SOPT of Berrington, Bransden, and Coleman [20], EBSM of Byron and Joachain [33], Glauber of Franco [18], and Born of Kim and Inokuti [17].

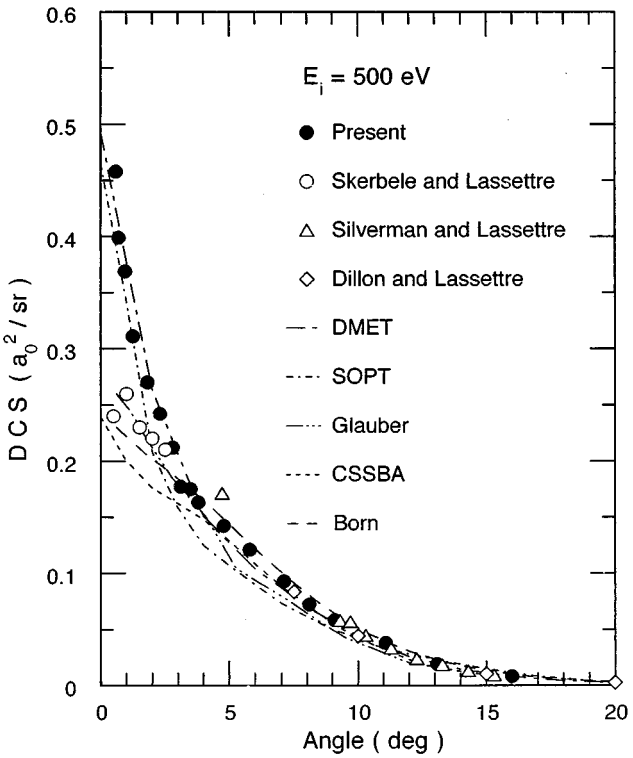

FIG. 7. The DCS's $(d\varsigma/d\Omega)_{2\,^1S}$ in He as a function of the scattering angle for the impact energy $E_i = 500$ eV. Experimental data of Skerbele and Lassettre [2], Silverman and Lassettre [1], and Dillon and Lassettre [8] are also plotted. Results of theoretical calculations are, in the order of the DCS value at $\theta = 0°$; DMET of Mansky and Flannery [21], SOPT of Berrington, Bransden, and Coleman [20], Glauber of Franco [18], CSSBA of Buckley and Walters [34], and Born of Kim and Inokuti [17].

smallest angles in agreement with the experimental results. We have made no attempt to evaluate the approximation methods, however, it is notable that the EBSM by Byron and Joachain reproduces the experimental data very closely.

In Fig. 7, the DCS's for the $2\,^1S$ excitation for the impact energy 500 eV are plotted in linear scale as a function of the scattering angle. Experimental data of Skerbele and Lassettre [2], Silverman and Lassettre [1], and Dillon and Lassettre [8] are also plotted. Although experimental data sets agree well at angles larger than 2°, there is a notable discrepancy between the present results and the data of Skerbele and Lassettre at the angles from 0.5° to 2.5°, which are the only other experimental data presently available for minute angles. The present results show a steep increase in the DCS at angles smaller than 2°, while the data of Skerbele and Lassettre do not show a forward peaking feature in the angular dependence of the DCS.

We have no basis from which to discuss the origin of the discrepancy of the data of Skerbele and Lassettre with the present ones, because no description is given on details of the calibration of the angle scale and the estimation of the angular resolution in their paper [2]. It is, however, worth noting that the general trend in cross section measured by Skerbele and Lassettre is consistent with ours if we assume their measurements were made with a somewhat worse angular resolution, with no correction of the type described in the Appendix being performed.

Theoretical calculations by the multichannel eikonal theory with the dipole correction (DMET) of Mansky and Flannery [21], and by the second-order potential theory of Berrington, Bransden,and Coleman [20] reproduce the forward peaking feature. However, the Glauber approximation of Franco [18], and the corrected simplified second Born approximation (CSSBA) of Buckley and Walters [34] do not reproduce the forward peaking behavior in the angular dependence of the DCS any better than the first Born approximation [17].

From comprehensive consideration of the experimental results and their comparison with theoretical calculations, we deduce the following features in the behavior of the DCS for the $2\,^1S$ excitation at small scattering angles: a forward peaking behavior is observed for the impact energies higher than 200 eV, and the steepness of the increase in the DCS at the smallest angles has a tendency to increase as the impact energy increases.

Elaborate theoretical calculations which include higher-order terms and take into account the contributions of several bound states reproduce the sharp increase in the DCS at minute scattering angles in a good agreement with the present experimental results. Intuitively, a contribution of the intermediate $2\,^1P$ state in the $2\,^1S$ excitation process is considered to be a main origin of the increase in the DCS at minute angles.

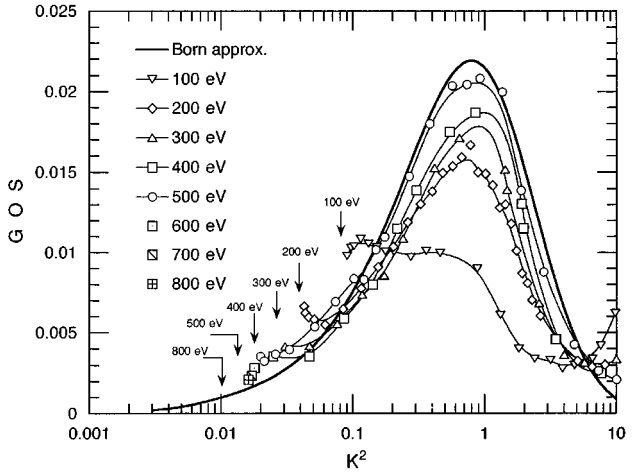

FIG. 8. The effective GOS, $F(K)$, for the excitation of the $2\,^1S$ state in He as functions of the squared momentum transfer K^2 for the impact energies $E_i=100$, 200, 300, 400, and 500 eV. The effective GOS's for $E_i=600$, 700, and 800 eV at the low limit of K^2 (for a measured angle of 0°, corresponding to a mean scattering angle of 0.6°) are also shown. A curve calculated by the first Born approximation is drawn using a thick line. Vertical arrows designated by the energy values indicate the minimum possible values of K^2 (for $\theta=0°$) for the respective impact energies.

The effective or apparent, GOS's, $F(K)$, for the $2\,^1S$ state are plotted in Fig. 8 as functions of the squared momentum transfer K^2 for impact energies $E_i=100$, 200, 300, 400, and 500 eV, while the effective GOS's for $E_i=600$, 700, and 800 eV are plotted only for $\theta=0°$ equivalent to a mean scattering angle $\theta=0.6°$. A curve of the GOS against K^2 calculated by the first Born approximation of Kim and Inokuti [17] is compared with the curves of the effective GOS's which are drawn for different impact energies. The curves of the effective GOS reveal a distinct variation depending on the impact energy. In particular, the effective GOS for the impact energy 100 eV behaves in a totally different way from those for higher impact energies. The effective GOS has a broad and flat minimum of about 0.003 at $K^2=2-6$, and increases up to $F=0.01$, nearly 50% larger in value than the first Born approximation, as K^2 decreases to $K^2=0.09$. The curves of the effective GOS for impact energies higher than 200 eV have their maxima at around $K^2=0.7-1.0$, and their overall heights become closer to the curve of the Born approximation as the impact energy increases, although the approach is very slow. The effective GOS curve for the impact energy 500 eV, for instance, is observed to be very close to the Born curve except for the region of K^2 smaller than 0.05 and for the region of K^2 larger than about 6.

Recent results of the effective GOS's determined by Xu, Feng, Wu, Ji, Zhang, Zhong, and Zheng [11] for the impact energy 1500 eV give excellent agreement with the GOS calculated by the first Born approximation within the experimental uncertainties, 8%, in the range of K^2 from 0.139 to 4.40.

The effective GOS curves against K^2 for different impact energies suggest the following features in the $2\,^1S$ excitation process. The curves approach the Born curve as the impact energy increases. The curve of effective GOS approaches the Born curve very slowly in contrast to the case for the $2\,^1P$ excitation [3]. Secondly, the GOS's do not agree with the Born GOS in the limit of small K^2, even if the impact energy is high enough for the first Born approximation to hold, as observed for the impact energies from 200 to 800 eV.

B. DCS for the $3\,^1S$ excitation

Experimental results of the scattering intensity ratios $(I_{3\,^1S}/I_{2\,^1P})$ and the DCS's $(d\sigma/d\Omega)_{3\,^1S}$ for the $3\,^1S$ excitation are tabulated in Table III for the impact energies 100, 200, 300, 400, and 500 eV. The corresponding GOS's $F(K)$ and the squared momentum transfer K^2 are also tabulated in the last two columns. The DCS's for the $2\,^1P$ excitation, which were employed as the normalized standards for the absolute scale, are also given in the third column. These DCS's are obtained in the same way as those described in Sec. II. The measurements were performed at the range of the scattering angle from about 1° to 15°, because it was practically impossible to discriminate the signals of the scattering intensity for the $3\,^1S$ excitation from the background noise at angles lower than 1°.

The experimental errors in the results of the DCS's for the $3\,^1S$ excitation are estimated to be about 15%, which is deduced as the quadratic sum of the statistical error of 10% in the intensity ratios, systematic error of 8% caused by the effect of the limited energy resolution, angular resolution, uncertainty in the angle calibration, etc., and the error of 7% in the absolute values of the $2\,^1P$ DCS, $(d\sigma/d\Omega)_{2\,^1P}$, used as the normalization standard. Again, a correction for the finite angular resolution was applied where necessary. The corrected results are presented in Table IV.

The scattering intensity ratio $(I_{3\,^1S}/I_{2\,^1P})$ is plotted in Fig. 9 as a function of the scattering angle for the different impact energies. The intensity ratio decreases rather steeply as the angle decreases from about 10° to the smallest angles, except for the curve for the impact energy $E_i=100$ eV. The steepness in this decrease became larger as the impact energy was increased. The overall tendency of the variation of the ratio with angle is similar to that for the $2\,^1S$ excitation, but the value of the ratio is about one order of magnitude smaller. The behavior in the variation of the ratios at the angles smaller than 1° to 2° is not clearly revealed here because of the lack of data at 0° and large statistical fluctuations in the ratio at minute angles.

The DCS's $(d\sigma/d\Omega)_{3\,^1S}$ are plotted in Figs. 10, 11, and 12 on a logarithmic scale as a function of the scattering angle for the impact energies 100, 200, and 500 eV, respectively. Theoretical calculations by means of the dipole corrected multichannel eikonal theory of Mansky and Flannery [21], the generalized distorted wave model (GDWM) of Winters, Issa, and Bransden [35], the distorted wave polarized orbital theory (DWPO) of Scott and McDowell [36] (not available for $E_i=500$ eV), and the first Born approximation of Kim and Inokuti [17], are shown for comparison.

As observed in Figs. 10 and 11, for the impact energies 100 and 200 eV, respectively, the DMET and the GDWM calculations appear to give the angular dependence of the DCS's which reproduce the experimental results relatively well, except for the data point at the angle 1.25° for the impact energy 100 eV, which may have a large fluctuation to

TABLE III. The intensity ratios $(d\sigma/d\Omega)_{3\,^1S}/(d\sigma/d\Omega)_{2\,^1P}$ and the DCS's $(d\sigma/d\Omega)_{3\,^1S}$ (in atomic units) at impact energies 100, 200, 300, 400, and 500 eV. The absolute cross sections for the $2\,^1P$ excitation $(d\sigma/d\Omega)_{2\,^1P}$, which are used for the normalization standards, are also listed. The squared momentum transfer K^2 and the corresponding effective generalized oscillator strengths $F(K)$ are listed in the last two columns. The square brackets denote powers of 10.

Scattering angle (deg)	Intensity ratio $\frac{(d\sigma/d\Omega)_{3\,^1S}}{(d\sigma/d\Omega)_{2\,^1P}}$	$(d\sigma/d\Omega)_{2\,^1P}$ (a_0^2/sr)	$(d\sigma/d\Omega)_{3\,^1S}$ (a_0^2/sr)	Squared momentum transfer K^2	Effective GOS for $3\,^1S$ $F(K)$
		$E_i = 100$ eV			
1	8.52[−3]				
2.2	1.06[−2]				
2.7	9.87[−3]				
3.7	1.04[−2]	3.92	4.07[−2]	1.36[−1]	2.66[−3]
4.7	1.03[−2]	3.29	3.39[−2]	1.53[−1]	2.48[−3]
5.7	9.96[−3]	2.71	2.70[−2]	1.73[−1]	2.25[−3]
6.7	1.02[−2]	2.21	2.25[−2]	1.98[−1]	2.13[−3]
7.7	1.06[−2]	1.78	1.88[−2]	2.26[−1]	2.04[−3]
9.7	1.31[−2]	1.15	1.50[−2]	2.94[−1]	2.12[−3]
11.7	1.52[−2]	7.46[−1]	1.14[−2]	3.78[−1]	2.06[−3]
13.7	2.02[−2]	5.00[−1]	1.01[−2]	4.77[−1]	2.31[−3]
		$E_i = 200$ eV			
1.75	4.38[−3]				
2.2	4.89[−3]				
3.2	5.28[−3]	6.37	3.36[−2]	9.44[−2]	1.42[−3]
4.2	5.98[−3]	4.41	2.63[−2]	1.26[−1]	1.48[−3]
5.2	8.00[−3]	3.06	2.45[−2]	1.65[−1]	1.81[−3]
6.2	1.10[−2]	2.14	2.35[−2]	2.13[−1]	2.24[−3]
8.2	1.71[−2]	1.09	1.86[−2]	3.34[−1]	2.78[−3]
10.2	2.88[−2]	5.71[−1]	1.65[−2]	4.88[−1]	3.60[−3]
11.2	3.77[−2]	4.17[−1]	1.57[−2]	5.78[−1]	4.07[−3]
13.2	5.29[−2]	2.25[−1]	1.19[−2]	7.82[−1]	4.17[−3]
15.2	6.59[−2]	1.22[−1]	8.06[−3]	1.02	3.68[−3]
		$E_i = 300$ eV			
0.75	3.75[−3]	1.92[+1]	7.17[−2]	3.71[−2]	1.17[−3]
1.75	3.13[−3]	1.23[+1]	3.85[−2]	5.32[−2]	8.98[−4]
2.75	4.67[−3]	7.24	3.38[−2]	8.23[−2]	1.22[−3]
3.75	6.93[−3]	4.36	3.01[−2]	1.24[−1]	1.64[−3]
4.75	9.20[−3]	2.71	2.49[−2]	1.79[−1]	1.96[−3]
5.75	1.30[−2]	1.75	2.28[−2]	2.47[−1]	2.46[−3]
7.75	2.30[−2]	7.79[−1]	1.80[−2]	4.21[−1]	3.32[−3]
9.75	3.95[−2]	3.71[−1]	1.46[−2]	6.46[−1]	4.14[−3]
14.75	1.02[−1]	6.19[−2]	6.34[−3]	1.43	3.97[−3]
		$E_i = 400$ eV			
2.75	5.25[−3]	6.77	3.55[−2]	9.06[−2]	1.40[−3]
3.75	6.99[−3]	3.71	2.59[−2]	1.47[−1]	1.65[−3]
4.75	1.19[−2]	2.16	2.57[−2]	2.21[−1]	2.46[−3]
5.75	1.79[−2]	1.31	2.34[−2]	3.12[−1]	3.15[−3]
7.75	3.54[−2]	5.14[−1]	1.82[−2]	5.46[−1]	4.33[−3]
9.75	5.92[−2]	2.16[−1]	1.27[−2]	8.49[−1]	4.69[−3]
14.75	1.73[−1]	2.66[−2]	4.59[−3]	1.91	3.79[−3]
		$E_i = 500$ eV			
1.2	2.09[−3]				
1.7	2.72[−3]				
2.3	3.55[−3]				
2.8	4.49[−3]				

TABLE III. (*Continued.*)

Scattering angle (deg)	Intensity ratio $\frac{(d\sigma/d\Omega)_{3\,^1S}}{(d\sigma/d\Omega)_{2\,^1P}}$	$(d\sigma/d\Omega)_{2\,^1P}$ (a_0^2/sr)	$(d\sigma/d\Omega)_{3\,^1S}$ (a_0^2/sr)	Squared momentum transfer K^2	Effective GOS for $3\,^1S$ $F(K)$
3.3	7.35[−3]	4.09	3.00[−2]	1.39[−1]	1.80[−3]
3.8	9.46[−3]	2.99	2.83[−2]	1.78[−1]	2.17[−3]
4.3	1.16[−2]	2.23	2.60[−2]	2.22[−1]	2.48[−3]
5.3	1.95[−2]	1.29	2.51[−2]	3.27[−1]	3.53[−3]
6.1	2.71[−2]	8.49[−1]	2.30[−2]	4.26[−1]	4.22[−3]
7.1	4.10[−2]	5.15[−1]	2.11[−2]	5.70[−1]	5.19[−3]
8.1	5.74[−2]	3.17[−1]	1.82[−2]	7.36[−1]	5.78[−3]
9.1	7.92[−2]	1.97[−1]	1.56[−2]	9.23[−1]	6.20[−3]
11.1	1.17[−1]	7.73[−2]	9.03 [3]	1.36	5.31[−3]
13.1	1.50[−1]	3.09[−2]	4.64[−3]	1.89	3.78[−3]

the minus side. As for the forward peaking tendency in the angular dependence of the DCS's for the impact energy 200 eV, which is anticipated from the analogy of the $2\,^1S$ case, it is not clear whether the forward peaking really occurs or not at angles smaller than 2°, because of the lack of data.

For the impact energy 500 eV, as Fig. 12 shows, the results of three kinds of calculation appear to reproduce the experimental data rather well. An indication of the existence of the forward peaking tendency in the DCS's is inferred at the smallest angles, in the same way as the case of the $2\,^1S$ excitation.

The effective GOS's, $F(K)$, for the $3\,^1S$ state are plotted in Fig. 13 as functions of the squared momentum transfer K^2 for the impact energies $E_i = 100$, 200, 300, 400, and 500 eV. The curves of the effective GOS versus K^2 behave very similarly to those for the $2\,^1S$ state and show a similar impact energy dependence. The effective GOS curves for the impact energies from 200 to 500 eV show similar shape as the Born curve having their maxima at around the K^2 of 0.6 to 0.8, and their overall height becomes closer to the Born curve as the impact energy increases. The curve for the impact energy 100 eV behaves in a quite different way from the other curves. The effective GOS increases as K^2 decreases up to nearly 0.003, which is more than 60% larger than that of the first Born approximation, at $K^2 \cong 0.11$ as the lowest limit of K^2.

TABLE IV. The DCS's $(d\sigma/d\Omega)_{3\,^1S}$ corrected for the limited angular resolution effects at small scattering angles, for impact energies 100, 200, and 500 eV. Average angles and absolute DCS's $(d\sigma/d\Omega)_{2\,^1P}$ for the $2\,^1P$ excitation corrected for the angular resolution effects are also listed. The squared momentum transfer K^2 and the effective GOS's $F(K)$ are listed corresponding to the corrected average angle and the corrected DCS's $(d\sigma/d\Omega)_{3\,^1S}$, respectively. See the Appendix for details of notation used in the headings of the second and third columns.

Measured angle θ_m (deg)	Mean scattering angle $\overline{\theta(\theta_m)}$ (deg)	$\int S(\theta_m,\theta_t) \times\left(\frac{d\sigma}{d\Omega}(\theta_t)\right)_{2\,^1P} d\theta_t$ (a_0^2/sr)	$\left(\frac{d\sigma}{d\Omega}[\overline{\theta(\theta_m)}]\right)_{3\,^1S}$ (a_0^2/sr)	Squared momentum transfer K^2	Effective GOS for $3\,^1S$ $F(K)$
		$E_i = 100$ eV			
1.2	1.25	4.98	4.23[−2]	1.13[−1]	2.30[−3]
2.2	2.20	4.57	4.84[−2]	1.19[−1]	2.76[−3]
2.7	2.70	4.34	4.28[−2]	1.24[−1]	2.55[−3]
		$E_i = 200$ eV			
1.75	1.75	1.013[+1]	4.44[−2]	6.41[−2]	1.27[−3]
2.2	2.20	8.92	4.36[−1]	7.16[−2]	1.40[−3]
		$E_i = 500$ eV			
1.2	1.25	2.093[+1]	4.37[−2]	3.68[−2]	6.94[−4]
1.8	1.8	1.387[+1]	3.77[−2]	5.52[−2]	8.97[−4]
2.3	2.3	9.42	3.34[−2]	7.76[−2]	1.12[−3]
2.8	2.8	6.43	2.89[−2]	1.05[−1]	1.31[−3]

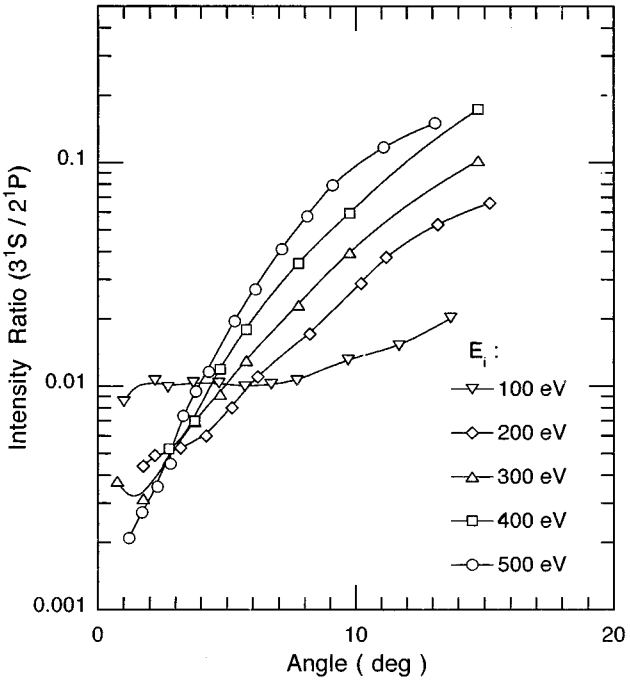

FIG. 9. Intensity ratio ($I_{3\,^1S}/I_{2\,^1P}$) in He as a function of the scattering angle for the impact energies $E_i = 100$, 200, 300, 400, and 500 eV.

The curves approach closer and closer to the Born curve as the impact energy increases, although the advance of the approach is very slow.

The effective GOS's appear to approach a larger value

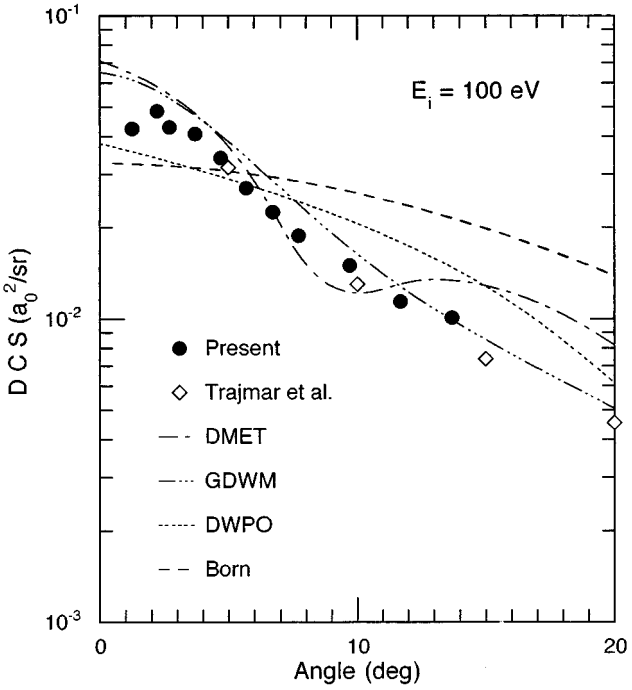

FIG. 10. The DCS's $(d\sigma/d\Omega)_{3\,^1S}$ in He as a function of the scattering angle for the impact energy $E_i = 100$ eV. Experimental data of Trajmar *et al.* [10] are also plotted. Results of the theoretical calculations are in the order of the DCS value at $\theta = 0°$. DMET of Mansky and Flannery [21], GDWM of Winters, Issa, and Bransden [35], DWPO of Scott and McDowell [36], and Born of Kim and Inokuti [17].

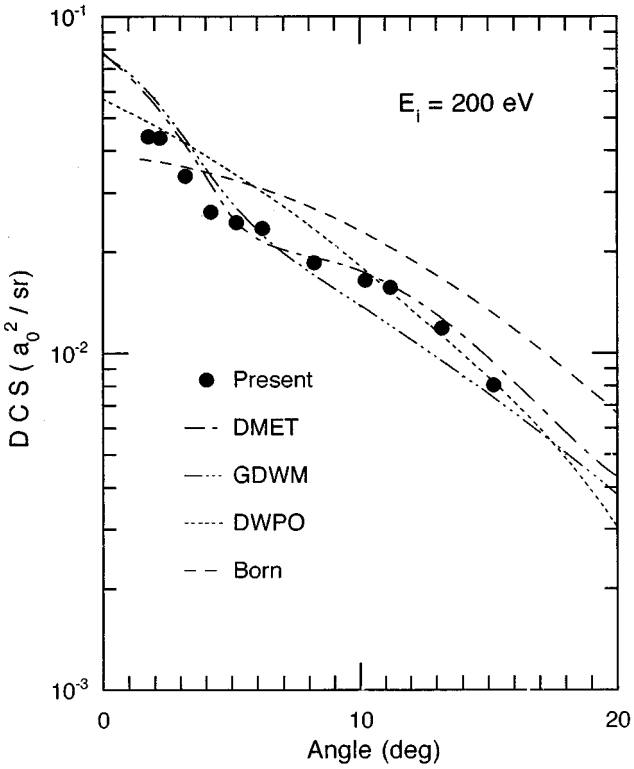

FIG. 11. The DCS's $(d\sigma/d\Omega)_{3\,^1S}$ in He as a function of the scattering angle for $E_i = 200$ eV. Results of the theoretical calculations are, in the order of the DCS value at $\theta = 0°$, DMET of Mansky and Flannery [21], GDWM of Winters, Issa, and Bransden [35], DWPO of Scott and McDowell [36], and Born of Kim and Inokuti [17].

than the theoretical GOS at the limit of the smallest K^2, although it is not clearly displayed for the curves of the impact energies 400 and 500 eV, due to the lack of data at the minute angles.

IV. SUMMARY

We have measured the DCS's for excitation of the $2\,^1S$ and $3\,^1S$ states from the ground state in He at scattering angles from 0° to 15° for the impact energies 100, 200, 300, 400, and 500 eV. We have paid special attention to performing the calibration of the true scattering angle and to keeping a relatively good angular resolution. The accuracy of the angle is estimated to be better than 0.2°, and the angular resolution is estimated to be 1.1° (FWHM) at angles from 0° to 3°, and 0.4° (FWHM) at angles larger than 3° and for the entire angular range for impact energies 300 and 400 eV.

Accuracy of determination of the DCS's for the $2\,^1S$ excitation is better than $\pm 11\%$ at angles larger than 3°, and is estimated to be $\pm 15\%$ at small angles.

Accuracy of the DCS's for the $3\,^1S$ excitation is also estimated to be $\pm 15\%$, and in this case no data were obtained at angles below 1° because of the poor signal-to-noise ratio.

Angular dependence of the DCS's reveals a remarkable forward peaking feature at minute scattering angles for the impact energies higher than 200 eV, in accordance with the predictions by the advanced theoretical calculations includ-

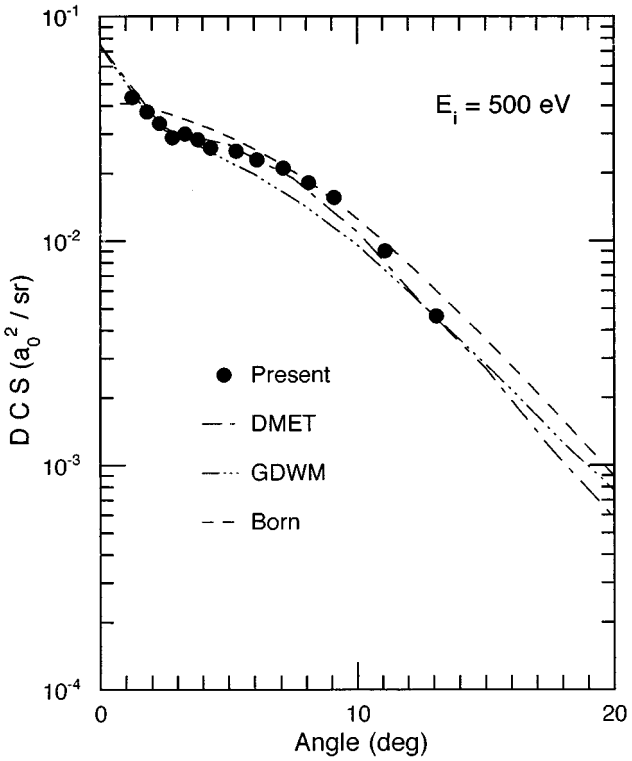

FIG. 12. The DCS's $(d\sigma/d\Omega)_{3\,^1S}$ in He as a function of the scattering angle for $E_i = 500$ eV. Results of the theoretical calculations are, in the order of the DCS value at $\theta = 0°$, DMET of Mansky and Flannery [21], GDWM of Winters, Issa, and Bransden [35], and Born of Kim and Inokuti [17].

ing higher-order terms and contributions of many bound states.

The curves of the GOS's as functions of the K^2 for different impact energies reveal the following features of this sort of transition. (1) The curve of the effective GOS approaches the curve calculated by the first Born approximation as the impact energy increases from 200 to 500 eV. (2) This approach is very slow, and the effective GOS's do not agree with the Born GOS even at the limit of the smallest K^2 up to the impact energy 800 eV for the $2\,^1S$ excitation.

This sort of feature in the curve of the effective GOS versus K^2 is characteristic of transitions where the term symbol is the same in the initial and final states. It is suggested that the feature of the curve of the effective GOS versus K^2 may help in identification of the character of unknown transitions which appear in the electron-energy-loss spectra of molecules.

We would like to emphasize that the measurement of the DCS's at minute scattering angles is important especially for optical forbidden transitions, because the knowledge of the behavior of the DCS's at minute angles is useful for testing the theoretical calculation methods. The experimental data are very scarce due to a technical difficulty in measurement of the electron-energy-loss spectra at 0° angle, because of the poor signal-to-noise ratio especially for forbidden transitions.

ACKNOWLEDGMENTS

We wish to thank Mrs. Ann Currell for helpful discussions in the presentation of this paper.

APPENDIX: CORRECTION FOR ANGULAR RESOLUTION EFFECTS

This paper is concerned with detection of electrons scattered through small angles. Under such circumstances, it is important to consider effects due to the finite angular resolution of the apparatus and systematic errors which arise when measuring the angular scale. These systematic errors and their treatment have been described in the main text.

Once the geometric scattering angle (i.e., the angle of intersection of the center lines of the final lens of the selector and the first lens of the analyzer) becomes comparable to the angular resolution of the device, the effect of integrating over a range of angles can no longer be ignored. To account for the range of scattering angles present in each measurement, we use a function $S(\theta_m, \theta_t)$ which describes the probability that for a geometric (or measured) scattering angle

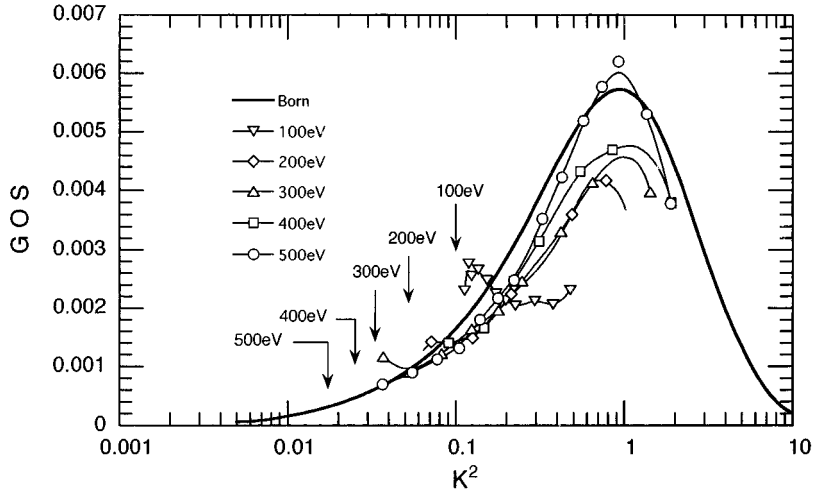

FIG. 13. The effective GOS, $F(K)$, for the excitation of the $3\,^1S$ state in He as functions of the squared momentum transfer K^2 for $E_i = 100$, 200, 300, 400, and 500 eV. A curve calculated by the first Born approximation is drawn using a thick line. Vertical arrows designated by the energy values indicate the minimum limit of K^2 (for $\theta = 0°$) for the respective impact energies.

θ_m, a detected scattering event was really due to scattering through an angle θ_t (i.e., the true scattering angle). As shown below, $S(\theta_m,\theta_t)$ can be calculated numerically subject to certain assumptions. Furthermore, $S(\theta_m,\theta_t)$ can then be used in subsequent equations to relate the actual measured intensity to a parametrization of the cross section [8]. In this way, we have accounted for the effects of finite angular resolution. The width of the distribution shown in Fig. 1 corresponds to $S(\theta_m,0)$ since this measurement was taken with no target gas to produce any scattering. Hence this distribution can be used to assess the function $S(\theta_m,\theta_t)$.

In considering the effects of the finite angular resolution of the selector and analyzer, we have assumed all the angles involved are small, making use of the approximations, $\sin\theta=\theta$ and $\cos\theta=1-\theta$. Furthermore, we assumed that angular distribution of the beam emerging from the selector and the efficiency of the analyzer have a Gaussian form. Accordingly, the expected intensity of a small part of the electron beam emerging from the interaction region is given by

$$P_s(\theta_s,\phi_s)=N_s\,\exp\left[\frac{-\theta_s^2-\phi_s^2}{2\sigma_s^2}\right], \tag{A1}$$

where N_s is a normalization factor, θ_s is the angle in the scattering plane measured with respect to the selector's beam axis, ϕ_s is the angle perpendicular to the scattering plane, and σ_s is a measure of the angular range produced by the selector system.

Similarly, the angular distribution of electrons entering the analyzer and subsequently resulting in detected events is

$$P_a(\theta_a,\phi_a,\theta_m)=N_a\,\exp\left[\frac{-(\theta_a-\theta_m)^2-\phi_a^2}{2\sigma_a^2}\right], \tag{A2}$$

where N_a is a normalization factor, θ_a is the angle in the scattering plane measured with respect to the analyzer's beam axis, ϕ_a is the angle perpendicular to the scattering plane, and σ_a is a measure of the analyzer's angular acceptance. θ_m is the angle which the center line of the selector's final lens system makes with the center line of the analyzer's first lens system. This angle corresponds to the measured scattering angle in the absence of systematic alignment errors.

We have ignored the finite size of the target region in this analysis. In practice, effects due to the size of the target region manifested as a path length correction have much less effect on the range of scattering angles accepted for a localized target of the type we used. The path length correction has been implicitly accounted for in our treatment of the experimental data since a reference cross section ($2\,^1P$) is used. This assumption is particularly valid for the spectrometers we used because the angular acceptance is defined by real apertures after the final lens system of the selector and before the input lens system of the analyzer.

We have approximated the number of electrons scattered through a scattering angle θ_t for some particular value of θ_m by

$$S(\theta_m,\theta_t)=\int_{4D}P_a(\theta_a,\phi_a,\theta_m)P_s(\theta_s,\phi_s)\,\delta(\theta_t,|\theta_s-\theta_a|+|\phi_s-\phi_a|)\,d\tau_{4D}, \tag{A3}$$

where the integral is over four angular dimensions given by

$$d\tau_{4D}=d\theta_a\,d\phi_a\,d\theta_s\,d\phi_s. \tag{A4}$$

The modulus terms in the δ function arise because the sign of the scattering angle has no meaning from the point of view of measured cross sections. The term $|\theta_s-\theta_a|+|\phi_s-\phi_a|$ is the absolute value of the scattering angle for small values of the angles θ_s, θ_a, ϕ_s, and ϕ_a.

The δ function in Eq. (A3) restricts the space over which the integral must be evaluated to a subspace of three dimensions. We can explicitly reduce this integral to a three-dimensional integral, removing one of the angular variables. Doing this, we get

$$S(\theta_m,\theta_t)=\int_{3D}P_s(\theta_s,\phi_s)G(\theta_a,\theta_t,\theta_s,\phi_s)\,d\tau_{3D}, \tag{A5}$$

where the integral is now over three angular dimensions given by

$$d\tau_{3D}=d\theta_a\,d\theta_s\,d\phi_s \tag{A6}$$

and the function $G(\theta_a,\theta_t,\theta_s,\phi_s)$ is given by

$$G(\theta_a,\theta_t,\theta_s,\phi_s)=P_a(\theta_a,+(\theta_t-|\theta_s-\theta_a|)-\phi_s,\theta_m)+P_a(\theta_a,-(\theta_t-|\theta_s-\theta_a|)-\phi_s,\theta_m). \tag{A7}$$

The angular profile shown in Fig. 1 can be calculated (except for the systematic shift which was subtracted during the data analysis) as $S(\theta_m,0)$. We use comparison between the measured profile and $S(\theta_m,0)$ to fix the parameters σ_a and σ_s. We made one further assumption to uniquely determine these parameters. Since the impact energy is almost equal to the collection energy and the geometry of the selector's last lens system is similar to the geometry of the analyzer's input lens system, we assumed $\sigma_s=\sigma_a$. Numerical experiments have shown that relaxation of this constraint makes little difference to the final results. Further numerical experiments have shown that the results have only a small dependence on the distributions used in Eqs. (A1) and (A2). An estimate of these effects has been included in the final uncertainties for the corrected results.

The function $S(\theta_m,\theta_t)$ was calculated by numerical integration for all values of θ_m at which measurements were made. As expected, these calculations showed that at low scattering angles, the average scattering angle is somewhat higher than the measured scattering angle. At higher scattering angles the difference becomes negligible.

A correction factor can be applied to the data, based on a known cross section as indicated by Eq. (1). The function $S(\theta_m,\theta_t)$ was used to relate the actual cross sections (in the limit of infinitesimal resolution) to the measured intensities. When this is done, the expression for correction becomes

$$\int S(\theta_m,\theta_t)\left(\frac{d\sigma}{d\Omega}(\theta_t)\right)_{2\,^1S} d\theta_t = \left(\frac{I_{2\,^1S}(\theta_m)}{I_{2\,^1P}(\theta_m)}\right)\int S(\theta_m,\theta_t)\left(\frac{d\sigma}{d\Omega}(\theta_t)\right)_{2\,^1P} d\theta_t, \quad \text{(A8)}$$

where the factors $I_{2\,^1S}(\theta_m)$, $I_{2\,^1P}(\theta_m)$, and $[(d\sigma/d\Omega)(\theta_t)]_{2\,^1P}$ are as defined in the main text with their functional dependencies now being made explicit. The reference data used to derive $[(d\sigma/d\Omega)(\theta_t)]_{2\,^1P}$ should be immune from angular resolution effects since it only concerns measurement at scattering angles greater than or equal to 7.5°. The right-hand side of Eq. (A8) can be written as a single function of θ_m. Hence,

$$g(\theta_m)=\left(\frac{I_{2\,^1S}(\theta_m)}{I_{2\,^1P}(\theta_m)}\right)\int S(\theta_m,\theta_t)\left(\frac{d\sigma}{d\Omega}(\theta_t)\right)_{2\,^1P} d\theta_t. \quad \text{(A9)}$$

This function can be evaluated numerically for any value of θ_m at which the two intensities have been measured at energies where the $2\,^1P$ cross section has been parametrized. From Eqs. (A8) and (A9) we have

$$g(\theta_m)=\int S(\theta_m,\theta_t)\left(\frac{d\sigma}{d\Omega}(\theta_t)\right)_{2\,^1S} d\theta_t, \quad \text{(A10)}$$

the right-hand side of which can be expanded as a Taylor's series, using moment integrals of the form

$$M_i=\int [\theta_t-\overline{\theta}(\theta_m)]^i S(\theta_m,\theta_t)\,d\theta_t \quad \text{(A11)}$$

to give

$$g(\theta_m)=\sum_i \frac{M_i}{i!}\frac{\partial^i}{\partial\theta^i}\left(\frac{d\sigma}{d\Omega}[\overline{\theta}(\theta_m)]\right)_{2\,^1S}, \quad \text{(A12)}$$

where $\overline{\theta}(\theta_m)$ is uniquely defined by the condition $M_1=0$. Hence, we see that $\overline{\theta}(\theta_m)$ is the mean scattering angle when the spectrometer is positioned at a measured scattering angle θ_m. For high angles, as expected, the condition $\overline{\theta}(\theta_m)\approx\theta_m$ was found to hold. The product of the two normalization constants N_s and N_a was fixed so that the condition $M_0=1$ holds, consistent with the interpretation that $S(\theta_m,\theta_t)$ is a probability distribution. In actual fact that subsequent analysis is independent of this condition since the normalization simply scales both sides of Eq. (A8).

Substituting these values and keeping terms up to $i=2$, we have

$$g(\theta_m)=\left(\frac{d\sigma}{d\Omega}[\overline{\theta}(\theta_m)]\right)_{2\,^1S}+\frac{M_2}{2}\frac{\partial^2}{\partial\theta^2}\left(\frac{d\sigma}{d\Omega}[\overline{\theta}(\theta_m)]\right)_{2\,^1S}. \quad \text{(A13)}$$

The second moment integral was calculated numerically and an estimate of the magnitude of the second differential of the cross section with respect to angle has been made from the experimental data. These calculations show that the experimental errors associated with the measurements are larger than the second term in this expression for $g(\theta_m)$. Hence, to the accuracy of the measurements presented in this paper, we have

$$g(\theta_m)=\left(\frac{d\sigma}{d\Omega}[\overline{\theta}(\theta_m)]\right)_{2\,^1S}. \quad \text{(A14)}$$

This equation simply shows us that the quantity $g(\theta_m)$ is equal to the cross section, not at the measured scattering angle but at the mean scattering angle calculated by integrating over all possible detected events.

Using Eq. (A9) and the condition that $M_1=0$, a table with entries $\overline{\theta}(\theta_m)$ and $(d\sigma/d\Omega)[\overline{\theta}(\theta_m)]_{2\,^1S}$ can be created with one entry for each measured scattering angle θ_m. Such a table has been created for all data which have systematic errors due to finite angular resolution which are comparable to the statistical errors of the measurements. Results are shown in Table II for the $2\,^1S$ excitation and in Table IV for the $3\,^1S$ excitation. Entries from these tables were used to replace uncorrected entries in all figures.

[1] S. M. Silverman and E. N. Lassettre, J. Chem. Phys. **40**, 1265 (1964).
[2] A. Skerbele and E. N. Lassettre, J. Chem. Phys. **45**, 1077 (1966).
[3] L. Vriens, J. A. Simpson, and S. R. Mielczarek, Phys. Rev. **165**, 7 (1968).
[4] G. E. Chamberlain, S. R. Mielczarek, and C. E. Kuyatt, Phys. Rev. A **2**, 1905 (1970).
[5] A. Yagishita, T. Takayanagi, and H. Suziki, J. Phys. B **9**, L53 (1976).
[6] H. Suzuki, T. Takayanagi, and K. Wakiya, Progress Report No. 2, Institute of Space and Aeronautical Science, University of Tokyo, 1974 (unpublished).
[7] T. Takayanagi, Ph.D. thesis, Sophia University, 1974 (in Japanese).
[8] M. A. Dillon and E. N. Lassettre, J. Chem. Phys. **62**, 2373 (1975).
[9] S. Trajmar, Phys. Rev. A **8**, 191 (1973).
[10] S. Trajmar, D. F. Register, D. C. Cartwright, and G. Csanak, J. Phys. B **25**, 4889 (1992).
[11] K. Z. Xu, R. F. Feng, S. L. Wu, Q. Ji, X. L. Zhang, Z. P. Zhong, and Y. Zheng, Phys. Rev. A **53**, 3081 (1996).
[12] H. Bethe, Ann. Phys. (Leipzig) **5**, 325 (1930).
[13] E. N. Lassettre, J. Chem. Phys. **53**, 3801 (1970).
[14] A. Skerbele and E. N. Lassettre, J. Chem. Phys. **53**, 3806 (1970).
[15] E. N. Lassettre and A. Skerbele, J. Chem. Phys. **54**, 1597 (1971).
[16] S. Nakazaki, in *Advances in Atomic, Molecular, and Optical Physics*, edited by Sir D. Bates and B. Bederson (Academic, New York, 1993), Vol. 30, pp. 1–44.
[17] Y. K. Kim and M. Inokuti, Phys. Rev. **175**, 176 (1968).
[18] V. Franco, Phys. Rev. A **8**, 2927 (1973).
[19] F. W. Byron, Jr. and C. J. Joachain, Phys. Rep., Phys. Lett. **34C**, 233 (1977).

[20] K. A. Berrington, B. H. Bransden, and J. P. Coleman, J. Phys. B **6**, 436 (1973).
[21] E. J. Mansky and M. R. Flannery, J. Phys. B **23**, 4573 (1990).
[22] W. C. Fon, K. A. Berrington, and A. E. Kingston, J. Phys. B **13**, 2309 (1980).
[23] G. P. Li, T. Takayanagi, K. Wakiya, H. Suzuki, T. Ajiro, S. Yagi, S. S. Kano, and H. Takuma, Phys. Rev. A **38**, 1240 (1988).
[24] T. Takayanagi, G. P. Li, K. Wakiya, H. Suzuki, T. Ajiro, T. Inaba, S. S. Kano, and H. Takuma, Phys. Rev. A **41**, 5948 (1990).
[25] T. Y. Suzuki, Y. Sakai, B. S. Min, T. Takayanagi, K. Wakiya, H. Suzuki, T. Inaba, and H. Takuma, Phys. Rev. A **43**, 5867 (1991).
[26] T. Y. Suzuki, H. Suzuki, F. J. Currell, S. Ohtani, T. Takayanagi, and K. Wakiya, Phys. Rev. A **53**, 4138 (1996).
[27] T. Y. Suzuki, H. Suzuki, S. Ohtani, B. S. Min, T. Takayanagi, and K. Wakiya, Phys. Rev. A **49**, 4578 (1994).
[28] Y. Sakai, T. Y. Suzuki, B. S. Min, T. Takayanagi, K. Wakiya, H. Suzuki, S. Ohtani, and H. Takuma, Phys. Rev. A **43**, 1656 (1991).
[29] K. Jost, J. Phys. E **12**, 1006 (1979).
[30] R. H. Jansen, F. J. de Heer, H. J. Luyken, B. van Wingerden, and H. J. Blaauw, J. Phys. B **9**, 185 (1976).
[31] D. C. Cartwright, G. Csanak, S. Trajmar, and D. F. Register, Phys. Rev. A **45**, 1602 (1992).
[32] D. Baye and P.-H. Heenen, J. Phys. B **7**, 938 (1974).
[33] F. W. Byron, Jr. and C. J. Joachain, J. Phys. B **8**, L284 (1975).
[34] B. D. Buckley and H. R. Walters, J. Phys. B **8**, 1693 (1975).
[35] K. H. Winters, M. Issa, and B. H. Bransden, Can. J. Phys. **55**, 1074 (1977).
[36] T. Scott and M. R. C. McDowell, J. Phys. B **9**, 2235 (1976).